DNAJB6a deficiency induces tau pathology through IRE1α-Xbp1-induced mitochondria dysfunction

Xiu Chen[1], Fang-Yuan Qian[1], Na Zhao[1], Xue-Ting Liu, Yan-Juan Wang, Fan Geng, Meng-Meng Zhu, Zhi-Jun Zhang, Qing-Guo Ren[*]

Department of neurology, Zhongda Hospital, School of Medicine, Jiangsu Provincial Key Laboratory of Brain Science and Medicine, Southeast University, Nanjing, 210009, China.

[1]These authors contributed equally.

Correspondence should be addressed to:

Qing-Guo Ren Ph.D.

Email: renqingguo1976@163.com

Tel: +86-25-83262255

Fax: +86-25-83262255

Funds: This study was supported by grants from the National Natural Science Foundation of China (NO. 81870850 and NO. 82001336) and the Postgraduate Research & Practice Innovation Program of Jiangsu Province (KYCX23_0322).

Science Press

ZR Zoological Research

Abstract

Endoplasmic reticulum (ER) stress and mitophagy have been indicated in the early stage of Alzheimer's disease (AD), in which tau hyperphosphorylation is one major pathological alteration. However, the precise mechanism remains unclear. Herein, the study identifies a crucial protein, the DnaJ (Hsp40) homolog, subfamily B, member 6a (DNAJB6a), and elucidates its potential pathogenic role in AD. The DNAJB6 gene is systematically screened using bioinformatics methods, confirming its decreased expression in AD patients' brains. And decreased DNAJB6a was found in the brains of the APP/PS1 mice compared to the control mice. DNAJB6a-/- mice exhibited cognitive impairment, synaptic loss and the pathological phenotypes of AD. Depletion of DNAJB6a led to activated ER stress depending on the downregulation of heat shock 70kDa protein 5 (HSPA5). Furthermore, DNAJB6a deficiency induced and accelerated AD-like phenotypes through activating IRE1α-XBP1 induced mitochondria dysfunction. These findings highlight DNAJB6a as a potential key target for preventing AD pathology.

Keywords:

DNAJB6; IRE1α-Xbp1; Alzheimer's disease; mitophagy; tau

Introduction

Alzheimer's disease (AD) is a condition that involves the buildup of protein clumps in the brain, including extracellular β-amyloid aggregates and intracellular

hyperphosphorylated tau aggregates(De Strooper and Karran, 2016; Knowles et al., 2014; Selkoe and Hardy, 2016). While the characteristics of this illness are well understood, it is widely acknowledged that the accumulation of protein deposits is linked to the disruption of the proteostasis network (PN)(Hipp et al., 2014; Morimoto and Cuervo, 2014).

Molecular chaperones and co-chaperones play a key role in the PN by controlling the folding conditions within cells, avoiding misfolding, and guiding nonnative intermediates towards their natural state(Hartl et al., 2011). Proteins can be cleared through the ubiquitin-proteasome system and autophagy(Schmidt and Finley, 2014). Heat shock proteins (HSPs) are universally present chaperone molecules categorized into various groups based on their size, such as HSPs like HSP40, HSP60, HSP70, HSP90, and HSP110, determined by their molecular mass (Vos et al., 2008; Wu et al., 2017). Numerous indications point to the involvement of HSPs in metabolic processes and the accumulation of both Aβ and Tau(Walls et al., 2012).

The HSP40 (DNAJ) family of co-chaperones is of particular interest in the context of proteotoxic neurodegeneration for several reasons. First, they act as critical specificity factors for HSP70 chaperones, often being the primary entities that recognize and bind to non-native proteins, thereby directing HSP70 activity to specific substrates(Moll et al., 2022; Zatsepina et al., 2021). More importantly, beyond this general role, numerous DNAJ members have demonstrated a direct ability to counteract the aggregation of key AD pathogenic proteins (Fayazi et al., 2006; Gillis et al., 2013; Hageman et al., 2010; Zijlstra et al., 2010). For instance, while DNAJB1 and DNAJC10 have been shown to

Science Press
ZR Zoological Research

inhibit Aβ oligomerization (Evans et al., 2006; Munoz-Lobato et al., 2014; Tsou et al., 2015). Moreover, DNAJB6 and DNAJB1 can directly interact with tau and suppress its aggregation (Abisambra et al., 2012; Chang et al., 2023; Sahara et al., 2007). Finally, Brehme et al. have shown that the knockdown of DNAJA1 and DNAJA4 or the C. elegans homologs can increase the aggregation and toxicity of Aβ42(Brehme et al., 2014). Prior research has indicated the involvement of the HSP40 group in AD pathology, yet the specific mechanisms remain unclear. This direct, substrate-specific chaperone activity against the principal culprits of AD pathology distinguishes many HSP40 proteins and positions them as crucial nodes in the cellular defense network that fails in AD.

The endoplasmic reticulum (ER) is an important organelle involved in protein quality control and cellular homeostasis. The accumulation of unfolded proteins leads to an ER stress, followed by an adaptive response via the activation of the unfolded protein response (UPR), PKR-like ER kinase (PERK), inositol-requiring transmembrane kinase/endoribonuclease 1α (IRE1α) and activating transcription factor 6 (ATF6) pathways (Oakes and Papa, 2014). Neuronal cells are particularly sensitive to protein misfolding, consequently ER and UPR dysfunctions were found to be involved in many neurodegenerative diseases including Alzheimer's disease, Parkinson's disease, among others characterized by the accumulation and aggregation of misfolded proteins (Hetz and Saxena, 2017). UPR activation is an initial occurrence in the AD brain(Scheper et al., 2011). Meanwhile, UPR activation enhances autophagy, and LC3 levels are increased in neurons displaying UPR activation in the AD brain(Alam and Scheper,

Science Press ZR Zoological Research

2016). Additionally, UPR activation promotes autophagy, leading to elevated levels of LC3 in neurons exhibiting UPR activation in the AD brain. Autophagy serves as the primary degradational pathway subsequent to UPR activation in neuronal cells, suggesting a correlation between UPR activation and autophagic pathology in the AD brain. Several members of the HSP40 family participate in ER-associated folding (ERAF) and ER-associated degradation (ERAD) in response to the unfolded protein response(Houck et al., 2014; Ushioda et al., 2008). The mechanisms by which these events contribute to pathological changes in AD are not well understood.

DNAJB6, a member of the HSP40 family, is prominently expressed in the central nervous system and serves multiple functions in mammalian development, clearance of misfolded protein aggregates, and maintenance of neural cell self-renewal(Meng et al., 2016). DNAJB6 is present in two spliced isoforms distinguished by alternative C-termini. The full-length isoform, DNAJB6a (38 kDa), primarily localizes to the nucleus as a result of the presence of a C-terminal nuclear localization sequence. In contrast, the shorter isoform, DNAJB6b (27 kDa), lacks this localization signal and is predominantly found in the cytoplasm(Andrews et al., 2012). Our previous study found that DANJB6a downregulation led to the increase of damaged mitochondria and the accumulation of autophagy-related proteins in skeletal muscle cells(Qian et al., 2021). And a study showed that DNAJB6 was downregulated in AD patients(Brehme et al., 2014). Altogether these results suggested that DNAJB6a might play an important role in AD.

In the present study, we calculated differentially expressed genes (DEGs) between 98

Science Press ZR Zoological Research

control samples and 310 AD samples from the GSE33000 dataset. After comparing with the published dataset of an analysis of other AD-related(Brehme et al., 2014), six common DEGs were found. And only DNAJC5 and DNAJB6 were expressed in both GABAergic and Glutamatergic neurons among these DEGs. Therefore, based on its differential expression and neuronal relevance, we prioritized DNAJB6 for functional characterization to elucidate its potential role in AD pathology. The primary discovery of this study suggests that decreased levels of DNAJB6a play a significant role in inhibiting mitophagy and impairing mitochondrial function in Alzheimer's disease. Additionally, the removal of Xbp1 effectively reinstated mitophagy, resulting in improved mitochondrial function and ultimately alleviating the pathology of Alzheimer's disease. Mechanistically, DNAJB6a bounds to and further stabilizes HSPA5 expression, inactivating IRE1α-Xbp1 signaling, which impedes its mitochondrial translocation. These findings indicate that targeting DANJB6a-induced inhibition of mitophagy may hold promise for therapeutic intervention in AD.

Materials and methods

Mice. APP/PS1 mice were obtained from Jackson Laboratory (Shanghai, China). DNAJB6a Knockout (*DNAJB6a*$^{-/-}$) Mouse Generation and Genotyping: *DNAJB6a*$^{-/-}$ mice were generated by Shanghai Model Organisms Center, using a CRISPR/Cas9 based approach. The sequence information of gRNAs is as follows: Sequence(5' -3') gRNA1(TGTGAGCCTCAGCCCTCCCT…TGG); gRNA2 (ATGACAACTGACCT CTATAT…GGG). Southeast University provided a specific- pathogen-free

Science Press ZR Zoological Research

environment with suitable temperature (20-25 °C) and humidity (50 ± 5%). All mice were kept on a standard 12h light/12h dark cycle (lights on from 8:00 a.m. to 8:00 p.m.) and given access to food and water ad libitum. All animal experiments were approved by the Laboratory Animal Ethics Committee of the College of Medicine, Southeast University (No.20200418080).

Data Processing. The RNA gene expression profiles of GSE33000 (https://www.ncbi.nlm.nih.gov/geo/query/acc.cgi?acc=GSE33000) and GSE36980 (https://www.ncbi.nlm.nih.gov/geo/query/acc.cgi?acc=GSE36980) were obtained from the Gene Expression Omnibus (GEO) database for analysis of Alzheimer's disease (AD) and control samples. Normalization of gene expression profiles was performed using the normalize Between Arrays function in the limma package of R software (version 3.6.2) as described by Ritchie et al (Ritchie et al., 2015). Age and gender matching between cases and controls was conducted based on clinical data from previous studies (Lardenoije et al., 2015; Riedel et al., 2016), with the mean age of AD cases ranging from 60 to 100 years, and the mean age of nondementia was years (range: 60-106 years).

Neuron Culture and Lentivirus Transfection. Cultures of cortical neurons from embryonic C57BL/6 mice at E15–16 were established following the protocol outlined by Giordano and Costa(Giordano and Costa, 2011). Specifically, cortical tissue obtained from 8-10 E15-16 mice was dissected into small fragments and subjected to

Science Press ZR Zoological Research

enzymatic digestion using 5% trypsin/EDTA at 37 °C, followed by mechanical dissociation with siliconized Pasteur pipettes. The trypsin activity was halted by the addition of 1 mL of fetal bovine serum (FBS), and the resulting cell suspension was filtered through a 40μm mesh to obtain a homogeneous single-cell population. The cells were enumerated and seeded onto poly-d-lysine-coated circular glass slides in 12-well culture plates containing 500mL of DMEM medium lacking FBS. Following a 24-hour incubation period, the culture medium was replaced with Neurobasal media supplemented with 1% B27, L-glutamate, and 1% PS. Subsequently, half of the medium was refreshed every three days. After 7 days of culture, the primary neurons used for the subsequent experiments. Finally, primary neurons subjected to western blotting and immunofluorescence staining. Each condition was conducted in three biological replicates.

Lentivirus vectors targeting knockdown of DNAJB6a and Xbp1 were obtained from Shanghai Genechem. Specific short hairpin (sh)RNA sequences designed to target DNAJB6a (shRNA, 5′-GACCTCAGCAGGGCTCAAAGA-3′) were incorporated into the hU6-MCS-CBh-gcGFP-IRES-puromycin vector. Similarly, shRNA sequences targeting Xbp1 (shRNA, 5′-AAGGAAGAACCTGTAGAAGAT-3′) were integrated into the same vector. Lentivirus vectors containing non-targeting sequences were utilized as a negative control. The transfection efficiency was evaluated through western blot analysis. Lentivirus was utilized for inducing knockdown in neurons. The viral quantity was determined based on the optimal multiplicity of infection (MOI), and a serum-free medium containing virus and polybrene was applied to the cells for a 6-

Science Press ZR Zoological Research

hour incubation period. Subsequently, the medium was replaced with a regular medium, and the subsequent experiment was conducted 48 hours later.

Western blotting. The samples were lysed in Tris-HCl, NaCl, and EDTA (TNE) buffer, followed by immunoblotting of the protein lysates with specified antibodies. Co-immunoprecipitation was conducted by incubating 1 mg of protein lysates with 1-2 μg of specified antibodies or IgG, along with 25 μl of Protein G-Agarose beads (88803; Thermo Scientific Pierce) at 4°C overnight. The immunocomplexes were subsequently analyzed by immunoblotting, and the protein band intensity was quantified using ImageJ software.

Nucleocytoplasmic separation. Cells were harvested and washed with ice-cold phosphate-buffered saline (PBS) three times. Nucleocytoplasmic separation was performed by a Nuclear and Cytoplasmic Protein Extraction Kit (P0027, Beyotime) according to the manufacturer's protocol.

Cycloheximide protein turnover assay. A cycloheximide (CHX) chase assay was performed to assess protein stability. Primary neuron cells were transfected with either control shRNA or DNAJB6a shRNA for 48 h. Cells were treated with DMSO or 100 μg/mL cycloheximide (MCE, HY-12320) for the indicated time points and subjected to immunoblotting for HSPA5, DNAJB6a, and β-actin.

Science Press ZR Zoological Research

Immunofluorescent staining. The brain slices and cultured cells were fixed in 4% (vol/vol) paraformaldehyde for 30 minutes at room temperature, followed by permeabilization with 0.5% (vol/vol) Triton X-100 diluted in PBS solution. Non-specific binding sites were blocked by incubating the samples in 5% (wt/vol) BSA containing 0.1% Triton X-100 (vol/vol) for 30 minutes. Subsequently, the samples were incubated with primary antibodies at 4 °C overnight, washed three times in PBS, and then incubated with secondary antibodies conjugated to Alexa-Fluor 488 or 594 for 1 hour at 37 °C. Hoechst (1:1,000) was used to further stain the samples for 10 minutes after three PBS washes. A 50% glycerin-PBS (vol/vol) solution was used to mount the samples onto slides after they had been cleaned. A confocal microscope (Olympus BX60, Tokyo) was used to capture images of each slide.

Golgi staining and spine analyses. The brains of mice were dissected and processed using the FD Rapid Golgistain™ Kit (FD NeuroTechnologies, Shanghai, China) in accordance with the manufacturer's guidelines. Subsequently, slices were examined using a confocal microscope to capture images of Golgi-impregnated hippocampal CA1 pyramidal neurons. Z-stack-compressed TIFF files were then imported into ImageJ for analysis, where images were calibrated based on acquisition parameters and the number of spines was quantified.

Transmission electron microscopy. The culture medium of each group was poured out and 2.5% glutaraldehyde was added. After 1 h, scrape off the cells, centrifuge, and

Science Press
ZR Zoological Research

discard the supernatant; The cells in the tube were blown, then they were moved to a new 1.5 mL EP tube. After natural sedimentation for 1 h, the supernatant was cleared out, and 1 mL of 2.5% glutaraldehyde was added into the 1.5 mL EP tube along the tube wall, and then the fixation, dehydration, embedding, and solidification were to be carried out. Sections (7 nm) were performed using the LYCRA EMUC70 ultramicrotome, and the sections were double-stained with 72% uranium acetate-lead citrate and observed under HT7800 transmission electron microscopy (80 KV).

Statistics. The data presented in this study are expressed as mean ± standard error of the mean (s.e.m.). Statistical analyses were conducted using GraphPad Prism or Origin software. Specific details regarding the statistical methods employed for each comparison are provided in the text.

Results

DNAJB6a is downregulated in the brain of AD mice.

To establish the cellular context of HSP40 family members in relevant neuronal populations, we mined single-cell RNA sequencing data from the Allen Institute for Brain Science of sorted mouse cortical and hippocampal neurons. This analysis revealed that DNAJC5 and DNAJB6 are constitutively expressed in both GABAergic and Glutamatergic neurons (Fig. 1A), the principal cell types affected in AD. Meanwhile, we calculated DEGs between 98 control samples and 310 AD samples from the GSE33000 dataset. Ultimately, 29 DEGs, including 27 downregulated and 2

Science Press ZR Zoological Research

upregulated genes were identified from the dataset (Fig. S1A and Supplementary Table S1). Next, we compared these DEGs with the published dataset of an analysis of other AD-related(Brehme et al., 2014). Notably, six common DEGs were found (Fig. S1B). These DEGs were largely absent, whereas DNAJC5 and DNAJB6 were expressed in both GABAergic and Glutamatergic neurons (Fig. 1A). Recent studies have identified DNAJC5 encoding cysteine-string protein α (CSPα) as the disease-causing gene of a rare autosomal dominant human neurodegenerative diseases (ND) known as adult-onset neuronal ceroid lipofuscinosis (ANCL)(Noskova et al., 2011). Among these, DNAJB6 was selected for further investigation due to its significant downregulation in AD and its known constitutive expression in neurons, positioning it as a compelling candidate for a role in AD pathogenesis.

DNAJB6 mRNA expression was shown to be significantly lower in AD brain tissues across different datasets (Fig. 1B). We further examined the expression levels of DNAJB6 protein in 9-month-old APPswe/PS1dE9 (APP/PS1) mice. Interestingly, compared with WT littermates, the downregulation of DNAJB6a was observed in the hippocampus of APP/PS1 mice (Fig. 1C-D). Collectively, these findings support that there is a close relationship between DNAJB6a and AD.

Cognitive impairment, tau hyperphosphorylation and impaired synaptic plasticity were observed in *DNAJB6a*$^{-/-}$ mice.

To explore the role of DNAJB6a in AD pathogenesis, DNAJB6a knockout mice (*DNAJB6a*$^{-/-}$) were used in the following experiments, and the deletion of DNAJB6a in the *DNAJB6a*$^{-/-}$ mice was confirmed by western blotting (Fig. S1C). Meanwhile, we

Science Press ZR Zoological Research

have performed Morris Water Maze tests to assess spatial learning and memory of the 10-month-old DNAJB6a$^{-/-}$ mice. The results demonstrate that compared to the wild-type (DNAJB6a$^{+/+}$) littermates, the DNAJB6a$^{-/-}$ mice exhibited: significantly impaired learning during the training days, as indicated by a longer escape latency to find the hidden platform; and significantly impaired memory in the probe trial, as shown by the less time spent in the target quadrant where the platform was previously located (Fig. 2A-B). Tau hyperphosphorylation is an important hallmark of AD, we found that p-Thr231 and p- Ser396, Tau5 and Tau1 were increased in the cortex and hippocampus of 10-month-old *DNAJB6a*$^{-/-}$ mice compared with those in *DNAJB6a*$^{+/+}$ mice (Fig. 2C-F). However, there was no significant difference in the mRNA level of total tau was observed between the chronic sleep-deprived group and the control two groups (Fig. S1D). Next, we assessed the effects of DNAJB6a deletion on synaptic plasticity. The protein levels of PSD-93 and PSD-95, which are key scaffolding components at PSDs, were reduced in the brains of *DNAJB6a*$^{-/-}$ mice (Fig. 2G-H). Besides, golgi staining showed that the number of mature spines in the hippocampal region of *DNAJB6a*$^{-/-}$ mice was significantly decreased compared with the *DNAJB6a*$^{+/+}$ mice (Fig. 2I). In sum, these results indicated that DNAJB6a could play an important role in the tau pathology. In vitro, we cultured primary neurons to further study the role of DNAJB6a in tau phosphorylation. We observed a significant increase in the protein levels of p-Thr231, p- Ser396, Tau5 and Tau1 in DNAJB6a shRNA knockdown (shJb6a) primary neuron compared with control (Scr) (Fig. 2J-K). Then, the increased level of p- Thr231 was further confirmed by immunofluorescence staining in the shJb6a primary neuron

Science Press ZR Zoological Research

compared with Scr (Fig. 2L and Fig. S1E). The above results were consistent with those in vivo experiments.

DNAJB6a responded to ER stress via the regulation of HSPA5.

Considering that DNAJ family members are related to ER stress biological process, we next investigated the effect of DNAJB6a on ER stress. To induce ER stress, primary neurons were incubated separately with 1 μM thapsigargin (a potent and well-established inducer of endoplasmic reticulum stress, Tg) for 0h, 8h, 16h, and 24 h. We found that the expression of DNAJB6a was decreased after exposure to Tg treatment, whereas DNAJB6b was not significantly altered (Fig. 3A-B). At the same time, immunofluorescence results showed that the HSPA5, a master regulator for ER stress, expressed in both nucleus and cytoplasm in DMSO treatment group, whereas the expression of HSPA5 decreased in the nucleus and increased in the cytoplasm after exposure to Tg treatment. (Fig. 3C). Subsequently, an interaction between DANJB6a and HSPA5 was identified through the CoIP assay and a notable decrease in the interaction between DNAJB6a and HSPA5 was observed in the Tg treatment group. (Fig. 3D). Given the nuclear localization of DNAJB6a, we hypothesized that the translocation of HSPA5 to the nucleus is potentially facilitated through its interaction with DNAJB6a. Then we found the expression of HSPA5 decreased in shJb6a primary neurons compared with Scr (Fig. 3E-G). There was no change in the messenger RNA (mRNA) levels of HSPA5 between Scr and shJb6a (Fig. 3J). However, as observed in the Cycloheximide (CHX) chase experiments, the degradation of HSPA5 protein was

Science Press ZR Zoological Research

significantly accelerated in shJb6a primary neurons compared with Scr, indicating that DNAJB6a stabilizes the protein expression of HSPA5 (Fig. 3H-I). Additionally, immunofluorescence results showed that HSPA5 was decreased in nucleus shJb6a primary neurons compared with Scr (Fig. 3K). Altogether, DNAJB6a could contribute to the ER stress response by facilitating the stability and nuclear localization of HSPA5.

DNAJB6a deficiency dysregulates PERK, IRE1α UPR branches.

UPR is activated in response to ER stress which controls the expression of many Endoplasmic reticulum (ER)-associated degradation (ERAD) genes through three branches of the UPR signaling initiated by protein kinase RNA (PKR)-like ER kinase (PERK), activating transcription factor 6 alpha (ATF6α), and inositol-requiring kinase 1 (IRE1)(Hwang and Qi, 2018). Subsequently, we pondered upon how DNAJB6a responds to ER stress by regulating UPR. ATF6α was not differentially expressed in shJb6a primary neurons compared with Scr (Fig. 4D). However, PERK phosphorylation, as well as downstream signaling proteins, Bax, cleaved-caspase-3, and Chop were enhanced in shJb6a primary neurons compared with Scr (Fig. 4A-B). Strikingly, the IRE1α, XBP-1u and XBP-1s were significantly upregulated in shJb6a primary neurons compared with Scr (Fig. 4C). In all, our data indicates that the knockdown of DNAJB6a enhances the activity of the PERK-Chop and IRE1α-Xbp1 in response to ER stress.

In the unstressed ER lumen, HSPA5 binds to PERK, IRE1α, and ATF6α to inhibit their oligomerization and phosphorylation, whereas during ER stress, HSPA5 releases these

receptors leading to their activation(Bertolotti et al., 2000a). As observed in the CoIP assay, the interaction between IRE1α and HSPA5 was increased in shJb6a primary neurons compared with Scr, while the interaction between PERK and HSPA5 remained unchanged (Fig. 4F-H).

Elevated p-PERK and PERK that were observed in shJb6a primary neurons were reversed by knockdown of Xbp1 (Fig. 4I). The knockdown efficacy was validated with a western blotting analysis (Figure 4J). Simultaneously, the transmission electron microscopy provided substantiation of ER stress in shJb6a primary neurons compared with Scr, exemplified by the presence of edema in the ER. (Fig. 4L). The results indicated that DNAJB6a could regulate UPR via IRE1α-Xbp1 signaling pathway.

DNAJB6a deficiency hinders mitophagy by impairing mitochondrial and lysosomal fusion.

ER and mitochondria are structurally and functionally connected(De Brito and Scorrano, 2008; Dorn et al., 2015). Correspondingly, shJb6a primary neurons exhibited an increased number of damaged mitochondria (mitochondrial swelling and loss of mitochondrial cristae), compared to the Scr group (Fig. 5A). In addition, elevated p62, LC3-II/ I ratio, VDAC1 and decreased TOMM20 were found in shJb6a primary neurons (Fig. 5B-D). The immunofluorescence results demonstrated that the deletion of DNAJB6a has no impact on the recruitment of LC3 to damaged mitochondria, as evidenced by the co-localization of LC3 with the mitochondrial marker protein TOMM20 (Fig. 5E). The localization of Mito-Tracker Green (a mitochondrial probe)

Science Press ZR Zoological Research

and Lyso-Tracker Blue (a lysosome probe) exhibited a notable decrease in shJb6a primary neurons compared with Scr, which signified that the reduction of DANJB6a hindered the fusion process between damaged mitochondria and lysosomes (Fig. 5F). These results suggest that DANJB6a deficiency could inhibit mitophagy through impairing autophagosome-lysosome fusion process.

Xbp1 knockdown could rescue mitophagy deficiency and tau hyperphosphorylation induced by the deletion of DNAJB6a.

Given our observation that DNAJB6a deletion led to the activation of IRE1α-Xbp1 signaling pathway and inhibition of mitophagy, we next explored whether DNAJB6a knockdown mediates mitophagy via the activation of IRE1α-Xbp1 signaling pathway. Elevated LC3-II, LC3-II/LC3-I ratio, P62, VDAC1 and decreased TOMM20 that were observed in shJb6a primary neurons were reversed by knockdown of Xbp1(Fig. 6A-D). shXbp1 primary neurons exhibited a decreased number of damaged mitochondria in shJb6a primary neurons (Fig. 6E). Meanwhile, shJb6a primary neurons exhibited a notable decrease in the localization of Mito-Tracker Green and Lyso-Tracker Blue, which was also rescued by the knockdown of Xbp1 (Fig. 6F). These data indicated that Xbp1 downregulation could rescue mitochondrial autophagy inhibition induced by the deletion of DNAJB6a. Finally. we found that the upregulated protein levels of p-Thr231, p-Ser396, Tau1 and Tau5 in shJb6a primary neurons were rescued by the knockdown of Xbp1 (Fig. 6G-H).

In summary, these results indicated that mitophagy deficiency and tau

Science Press ZR Zoological Research

hyperphosphorylation induced by the deletion of DNAJB6a could be triggered by elevated IRE1α-Xbp1.

Discussion

Alzheimer's disease (AD) is a neurodegenerative disease associated with aging and is the primary cause of dementia in humans. In both aging and AD brains, there is a notable increase in the repression of heat shock proteins (HSPs) compared to the general repression of genes in the genome(Brehme et al., 2014). The pathophysiological mechanism of the link between reduced HSPs and AD remains unclear. In our study, we found that DNAJB6a was downregulated in the brains of AD patients and AD mice. And DNAJB6 was mainly expressed in the hippocampus and prefrontal cortex regions of mice, which participate in memory encoding and recalling. DNAJB6a deletion could cause synaptic plasticity impairment and tau hyperphosphorylation both in mice brain and primary culture neurons. Our results demonstrate that the degradation of steady-state HSPA5 is mediated by DNAJB6a, leading to the activation of IRE1α-Xbp1, therefore preventing mitophagy-mediated tau accumulation, suggesting its potential roles in the pathogenesis of AD.

Hyperphosphorylated tau is neurotoxic and aggregates to generate intracellular neurofibrillary tangles that pathologically appear in AD and other tauopathy illnesses(Takashima, 2008). Emerging research indicates that dysfunctions in mitochondrial and autophagic-lysosomal pathways may represent early indicators of Alzheimer's disease pathogenesis, contributing to the development of hallmark

Science Press ZR Zoological Research

397 pathologies(Kerr et al., 2017). Specifically, mitophagy has been shown to attenuate tau
398 pathology and ameliorate cognitive impairments in Alzheimer's disease models(Fang
399 et al., 2019). In AD brains, the levels of mitophagy are obviously decreased(Manczak
400 et al., 2018). Combined with western blot and electron microscopy results, damaged
401 mitochondria were found in DNAJB6a knockdown neurons in the present study.
402 Furthermore, our previous study found that the deletion of DANJB6a led to the increase
403 of damaged mitochondria and the accumulation of autophagy-related proteins in
404 skeletal muscle cells(Qian et al., 2021). These findings indicate that DNAJB6a can
405 regulate tau accumulation by modulating mitophagy.
406 Increasing evidence has shown that there is ER stress activation in the AD
407 brain(Hoozemans et al., 2009; Roussel et al., 2013). A recent study found that the hearts
408 of zebrafish lacking the DNAJB6a homolog show activation of the ER stress(Ding et
409 al., 2016). In the present study, we found that Tg caused ER stress activation in
410 accordance with a decreased level of DNAJB6a expression, whereas DNAJB6b was
411 not significantly altered in this process, suggesting that DNAJB6a but not DNAJB6b
412 plays an important role ER homeostasis. HSPA5/BiP or GRP78 is a molecular
413 chaperone protein predominantly in the ER lumen, that interacts with unfolded proteins
414 through its C-terminal substrate-binding domain(Bertolotti et al., 2000a). In our study,
415 we found that Tg could activate ER stress, decrease HSPA5 expression and change its
416 location (cytoplasmic translocation). Given the nuclear localization of DNAJB6a, we
417 speculate that DNAJB6a is involved in the activation of ER stress by interacting with
418 HSPA5. When DNAJB6a is decreased, the interaction between DNAJB6a and HSPA5

Science Press ZR Zoological Research

is decreased. HSPA5 was released from nucleus to cytoplasm, and ER stress was activated. We found that DNAJB6a did interact with HSPA5 under normal conditions. However, the protein interaction between DNAJB6a and HSPA5 was significantly reduced after ER stress activation. Besides cytoplasmic translocation, we also found that DNAJB6a deletion could decrease HSPA5 expression. Further research found that DNAJB6a deletion significantly accelerates HSPA5 degradation rather than affecting its protein synthesis, indicating that DNAJB6a participates in ER stress response through stabilizing HSPA5 post-translationally and nuclear localization.

In the absence of stress in the endoplasmic reticulum (ER) lumen, HSPA5 interacts with PERK and IRE1α, facilitating the activation of ATF6α while preventing their oligomerization and phosphorylation. Conversely, under conditions of ER stress, HSPA5 dissociates from these receptors, thereby promoting their activation(Bertolotti et al., 2000b). In our study, we found that both PERK and IRE1α were increased in DNAJB6a-shRNA neurons. DNAJB6a can stabilize HSPA5 post-translationally and nuclear localization, one possible mechanism is that DNAJB6a inhibits IRE1α and PERK activity and stabilizes the interaction between HSPA5 and IRE1α and PERK by increasing the substrate-binding ability of HSPA5, similar to ERdj4(Shen et al., 2002). Several reports have highlighted potential crosstalk between IRE1α and PERK signaling pathways(Lee et al., 2002). Our CoIP data demonstrated that DNAJB6a deletion only affects HSPA5 interacted with IRE1α, not PERK, infer that activation of the PERK signaling pathway is mediated by the IRE1α-Xbp1 signaling pathway in the DNAJB6a-shRNA primary neurons.

Science Press
ZR Zoological Research

IRE1α has both kinase and endonuclease activity. During ER stress, activated IRE1α splices Xbp1 mRNA to the mature form sXbp1(Cox and Walter, 1996). Indeed, our data demonstrated that DNAJB6a depletion led to the increased level of Xbp1, in accordance with increased IRE1α phosphorylation, suggesting that Xbp1 is regulated by IRE1α in shJb6a primary neurons.

Previous studies have detected that Xbp1 deficiency in the nervous system protects against amyotrophic lateral sclerosis by increasing autophagy(Hetz et al., 2009). The process of mitophagy is the recruitment of damaged mitochondria by LC3, and the recruited mitochondria combine with the fused medium for degradation. In our study, mitochondrial swelling and loss of mitochondrial cristae, elevated p62, LC3-II/ I ratio, VDAC1 and decreased TOMM20 were found in shJb6a primary neurons, supporting that the deletion of DNAJB6a could increase mitochondria impairment. No change was found in the co-localization of LC3 with the mitochondrial marker protein TOMM20 inferring that the deletion of DNAJB6a has no impact on the recruitment of LC3 to damaged mitochondria. However, the co-localization of mitochondria and lysosomes exhibited a notable decrease in shJb6a primary neurons, suggesting that the reduction of DANJB6a hindered the fusion process between damaged mitochondria and lysosomes. These results suggest that DANJB6a deficiency could inhibit mitophagy through impairing the autophagosome-lysosome fusion process.

Given that Xbp1 can inhibit the fusion of damaged mitochondria, which allows the mitochondria to be easily eliminated(Gustafsson, 2011). In our study, we found that impaired mitochondria, elevated LC3-II/LC3-I ratio, P62, VDAC1 and decreased

Science Press ZR Zoological Research

TOMM20 that were observed in shJb6a primary neurons were reversed by Xbp1 deletion. And the fusion of mitochondria and lysosomes was the same. Furthermore, we also found that Xbp1 deletion could reverse tau accumulation in shJb6a primary neurons. These data indicated that Xbp1 downregulation could rescue mitochondrial autophagy inhibition induced by the deletion of DNAJB6a.

In conclusion, DNAJB6a deficiency induces IRE1α-Xbp1 signal passageway upregulation, which impairs mitophagy, consequently leading to tau accumulation. These results suggested that DNAJB6a is a key modulator for mitochondria function and targeting DNAJB6a may therefore provide a therapeutic approach for AD.

Data availability. The datasets used and analysed during the current study are available from the corresponding author on reasonable request.

Competing interests

The authors have declared that no conflict of interest exists.

Authors' contributions

CX, QFY, ZN and RQG contributed to conception and design of the study, acquisition and analysis of data, and drafting the manuscript, LXT, WYJ, GF, ZMM and ZZJ contributed to acquisition and analysis of data.

Acknowledgements

Science Press
ZR Zoological Research

We thank Dr. Li zemin for her kind gift of xbp1 and perk antibodies.

References

Abisambra JF, Jinwal UK, Suntharalingam A, Arulselvam K, Brady S, Cockman M, et al. 2012. DnaJA1 antagonizes constitutive Hsp70-mediated stabilization of tau. *J Mol Biol*, **421**(4-5): 653-661.

Alam J & Scheper W. 2016. Targeting neuronal MAPK14/p38alpha activity to modulate autophagy in the Alzheimer disease brain. *Autophagy*, **12**(12): 2516-2520.

Andrews JF, Sykora LJ, Letostak TB, Menezes ME, Mitra A, Barik S, et al. 2012. Cellular stress stimulates nuclear localization signal (NLS) independent nuclear transport of MRJ. *Exp Cell Res*, **318**(10): 1086-1093.

Bertolotti A, Zhang Y, Hendershot LM, Harding HP, Ron D. 2000a. Dynamic interaction of BiP and ER stress transducers in the unfolded-protein response. *Nat Cell Biol*, **2**(6): 326-332.

Bertolotti A, Zhang Y, Hendershot LM, Harding HP, Ron D. 2000b. Dynamic interaction of BiP and ER stress transducers in the unfolded-protein response. *Nature Cell Biology*, **2**(6): 326-332.

Brehme M, Voisine C, Rolland T, Wachi S, Soper JH, Zhu Y, et al. 2014. A chaperome subnetwork safeguards proteostasis in aging and neurodegenerative disease. *Cell Rep*, **9**(3): 1135-1150.

Chang YL, Yang CC, Huang YY, Chen YA, Yang CW, Liao CY, et al. 2023. The HSP40 family chaperone isoform DNAJB6b prevents neuronal cells from tau aggregation.

BMC Biol, **21**(1): 293.

Cox JS & Walter P. 1996. A novel mechanism for regulating activity of a transcription factor that controls the unfolded protein response. *Cell*, **87**(3): 391-404.

De Brito OM & Scorrano L. 2008. Mitofusin 2 tethers endoplasmic reticulum to mitochondria. *Nature*, **456**(7222): 605-610.

De Strooper B & Karran E. 2016. The Cellular Phase of Alzheimer's Disease. *Cell*, **164**(4): 603-615.

Ding Y, Long PA, Bos JM, Shih YH, Ma X, Sundsbak RS, et al. 2016. A modifier screen identifies DNAJB6 as a cardiomyopathy susceptibility gene. *JCI Insight*, **1**(14).

Dorn GW, 2nd, Song M, Walsh K. 2015. Functional implications of mitofusin 2-mediated mitochondrial-SR tethering. *J Mol Cell Cardiol*, **78**: 123-128.

Evans CG, Wisen S, Gestwicki JE. 2006. Heat shock proteins 70 and 90 inhibit early stages of amyloid beta-(1-42) aggregation in vitro. *J Biol Chem*, **281**(44): 33182-33191.

Fang EF, Hou Y, Palikaras K, Adriaanse BA, Kerr JS, Yang B, et al. 2019. Mitophagy inhibits amyloid-beta and tau pathology and reverses cognitive deficits in models of Alzheimer's disease. *Nat Neurosci*, **22**(3): 401-412.

Fayazi Z, Ghosh S, Marion S, Bao X, Shero M, Kazemi-Esfarjani P. 2006. A Drosophila ortholog of the human MRJ modulates polyglutamine toxicity and aggregation. *Neurobiol Dis*, **24**(2): 226-244.

Gillis J, Schipper-Krom S, Juenemann K, Gruber A, Coolen S, Van Den Nieuwendijk R, et al. 2013. The DNAJB6 and DNAJB8 protein chaperones prevent intracellular aggregation of polyglutamine peptides. *J Biol Chem*, **288**(24): 17225-17237.

Science Press ZR Zoological Research

529 Giordano G & Costa LG. 2011. Primary neurons in culture and neuronal cell lines for
530 in vitro neurotoxicological studies. *Methods Mol Biol*, **758**: 13-27.
531 Gustafsson AB. 2011. Bnip3 as a dual regulator of mitochondrial turnover and cell
532 death in the myocardium. *Pediatric Cardiology*, **32**(3): 267-274.
533 Hageman J, Rujano MA, Van Waarde MA, Kakkar V, Dirks RP, Govorukhina N, et al.
534 2010. A DNAJB chaperone subfamily with HDAC-dependent activities suppresses
535 toxic protein aggregation. *Mol Cell*, **37**(3): 355-369.
536 Hartl FU, Bracher A, Hayer-Hartl M. 2011. Molecular chaperones in protein folding
537 and proteostasis. *Nature*, **475**(7356): 324-332.
538 Hetz C & Saxena S. 2017. ER stress and the unfolded protein response in
539 neurodegeneration. *Nature Reviews. Neurology*, **13**(8): 477-491.
540 Hetz C, Thielen P, Matus S, Nassif M, Court F, Kiffin R, et al. 2009. XBP-1 deficiency
541 in the nervous system protects against amyotrophic lateral sclerosis by increasing
542 autophagy. *Genes & Development*, **23**(19): 2294-2306.
543 Hipp MS, Park SH, Hartl FU. 2014. Proteostasis impairment in protein-misfolding and
544 -aggregation diseases. *Trends Cell Biol*, **24**(9): 506-514.
545 Hoozemans JJM, Van Haastert ES, Nijholt DaT, Rozemuller AJM, Eikelenboom P,
546 Scheper W. 2009. The unfolded protein response is activated in pretangle neurons in
547 Alzheimer's disease hippocampus. *The American Journal of Pathology*, **174**(4): 1241-
548 1251.
549 Houck SA, Ren HY, Madden VJ, Bonner JN, Conlin MP, Janovick JA, et al. 2014.
550 Quality control autophagy degrades soluble ERAD-resistant conformers of the

Science Press ZR Zoological Research

misfolded membrane protein GnRHR. *Molecular Cell*, **54**(1): 166-179.

Hwang J & Qi L. 2018. Quality Control in the Endoplasmic Reticulum: Crosstalk between ERAD and UPR pathways. *Trends In Biochemical Sciences*, **43**(8): 593-605.

Kerr JS, Adriaanse BA, Greig NH, Mattson MP, Cader MZ, Bohr VA, et al. 2017. Mitophagy and Alzheimer's Disease: Cellular and Molecular Mechanisms. *Trends Neurosci*, **40**(3): 151-166.

Knowles TP, Vendruscolo M, Dobson CM. 2014. The amyloid state and its association with protein misfolding diseases. *Nat Rev Mol Cell Biol*, **15**(6): 384-396.

Lardenoije R, Iatrou A, Kenis G, Kompotis K, Steinbusch HW, Mastroeni D, et al. 2015. The epigenetics of aging and neurodegeneration. *Prog Neurobiol*, **131**: 21-64.

Lee K, Tirasophon W, Shen X, Michalak M, Prywes R, Okada T, et al. 2002. IRE1-mediated unconventional mRNA splicing and S2P-mediated ATF6 cleavage merge to regulate XBP1 in signaling the unfolded protein response. *Genes Dev*, **16**(4): 452-466.

Manczak M, Kandimalla R, Yin X, Reddy PH. 2018. Hippocampal mutant APP and amyloid beta-induced cognitive decline, dendritic spine loss, defective autophagy, mitophagy and mitochondrial abnormalities in a mouse model of Alzheimer's disease. *Hum Mol Genet*, **27**(8): 1332-1342.

Meng E, Shevde LA, Samant RS. 2016. Emerging roles and underlying molecular mechanisms of DNAJB6 in cancer. *Oncotarget*, **7**(33): 53984-53996.

Moll A, Ramirez LM, Ninov M, Schwarz J, Urlaub H, Zweckstetter M. 2022. Hsp multichaperone complex buffers pathologically modified Tau. *Nat Commun*, **13**(1): 3668.

Science Press ZR Zoological Research

573 Morimoto RI & Cuervo AM. 2014. Proteostasis and the aging proteome in health and
574 disease. *J Gerontol A Biol Sci Med Sci*, **69 Suppl 1**(Suppl 1): S33-38.
575 Munoz-Lobato F, Rodriguez-Palero MJ, Naranjo-Galindo FJ, Shephard F, Gaffney CJ,
576 Szewczyk NJ, et al. 2014. Protective role of DNJ-27/ERdj5 in Caenorhabditis elegans
577 models of human neurodegenerative diseases. *Antioxid Redox Signal*, **20**(2): 217-235.
578 Noskova L, Stranecky V, Hartmannova H, Pristoupilova A, Baresova V, Ivanek R, et al.
579 2011. Mutations in DNAJC5, encoding cysteine-string protein alpha, cause autosomal-
580 dominant adult-onset neuronal ceroid lipofuscinosis. *Am J Hum Genet*, **89**(2): 241-252.
581 Oakes SA & Papa FR. 2014. The role of endoplasmic reticulum stress in human
582 pathology. *Annual Review of Pathology*, **10**: 173-194.
583 Qian FY, Guo YD, Zu J, Zhang JH, Zheng YM, Abdoulaye IA, et al. 2021. A novel
584 recessive mutation affecting DNAJB6a causes myofibrillar myopathy. *Acta*
585 *Neuropathol Commun*, **9**(1): 23.
586 Riedel BC, Thompson PM, Brinton RD. 2016. Age, APOE and sex: Triad of risk of
587 Alzheimer's disease. *J Steroid Biochem Mol Biol*, **160**: 134-147.
588 Ritchie ME, Phipson B, Wu D, Hu Y, Law CW, Shi W, et al. 2015. limma powers
589 differential expression analyses for RNA-sequencing and microarray studies. *Nucleic*
590 *Acids Res*, **43**(7): e47.
591 Roussel BD, Kruppa AJ, Miranda E, Crowther DC, Lomas DA, Marciniak SJ. 2013.
592 Endoplasmic reticulum dysfunction in neurological disease. *The Lancet. Neurology*,
593 **12**(1): 105-118.
594 Sahara N, Maeda S, Yoshiike Y, Mizoroki T, Yamashita S, Murayama M, et al. 2007.

Science Press
ZR Zoological Research

595 Molecular chaperone-mediated tau protein metabolism counteracts the formation of
596 granular tau oligomers in human brain. *J Neurosci Res*, **85**(14): 3098-3108.
597 Scheper W, Nijholt DA, Hoozemans JJ. 2011. The unfolded protein response and
598 proteostasis in Alzheimer disease: preferential activation of autophagy by endoplasmic
599 reticulum stress. *Autophagy*, **7**(8): 910-911.
600 Schmidt M & Finley D. 2014. Regulation of proteasome activity in health and disease.
601 *Biochim Biophys Acta*, **1843**(1): 13-25.
602 Selkoe DJ & Hardy J. 2016. The amyloid hypothesis of Alzheimer's disease at 25 years.
603 *EMBO Molecular Medicine*, **8**(6): 595-608.
604 Shen Y, Meunier L, Hendershot LM. 2002. Identification and characterization of a
605 novel endoplasmic reticulum (ER) DnaJ homologue, which stimulates ATPase activity
606 of BiP in vitro and is induced by ER stress. *The Journal of Biological Chemistry*,
607 **277**(18): 15947-15956.
608 Takashima A. 2008. Hyperphosphorylated tau is a cause of neuronal dysfunction in
609 tauopathy. *Journal of Alzheimer's Disease : JAD*, **14**(4): 371-375.
610 Tsou WL, Hosking RR, Burr AA, Sutton JR, Ouyang M, Du X, et al. 2015. DnaJ-1 and
611 karyopherin alpha3 suppress degeneration in a new Drosophila model of
612 Spinocerebellar Ataxia Type 6. *Hum Mol Genet*, **24**(15): 4385-4396.
613 Ushioda R, Hoseki J, Araki K, Jansen G, Thomas DY, Nagata K. 2008. ERdj5 is
614 required as a disulfide reductase for degradation of misfolded proteins in the ER.
615 *Science (New York, N.Y.)*, **321**(5888): 569-572.
616 Vos MJ, Hageman J, Carra S, Kampinga HH. 2008. Structural and functional diversities

Science Press ZR Zoological Research

between members of the human HSPB, HSPH, HSPA, and DNAJ chaperone families. *Biochemistry*, **47**(27): 7001-7011.

Walls KC, Coskun P, Gallegos-Perez JL, Zadourian N, Freude K, Rasool S, et al. 2012. Swedish Alzheimer mutation induces mitochondrial dysfunction mediated by HSP60 mislocalization of amyloid precursor protein (APP) and beta-amyloid. *J Biol Chem*, **287**(36): 30317-30327.

Wu J, Liu T, Rios Z, Mei Q, Lin X, Cao S. 2017. Heat Shock Proteins and Cancer. *Trends Pharmacol Sci*, **38**(3): 226-256.

Zatsepina OG, Evgen'ev MB, Garbuz DG. 2021. Role of a Heat Shock Transcription Factor and the Major Heat Shock Protein Hsp70 in Memory Formation and Neuroprotection. *Cells*, **10**(7).

Zijlstra MP, Rujano MA, Van Waarde MA, Vis E, Brunt ER, Kampinga HH. 2010. Levels of DNAJB family members (HSP40) correlate with disease onset in patients with spinocerebellar ataxia type 3. *Eur J Neurosci*, **32**(5): 760-770.

Science Press ZR Zoological Research

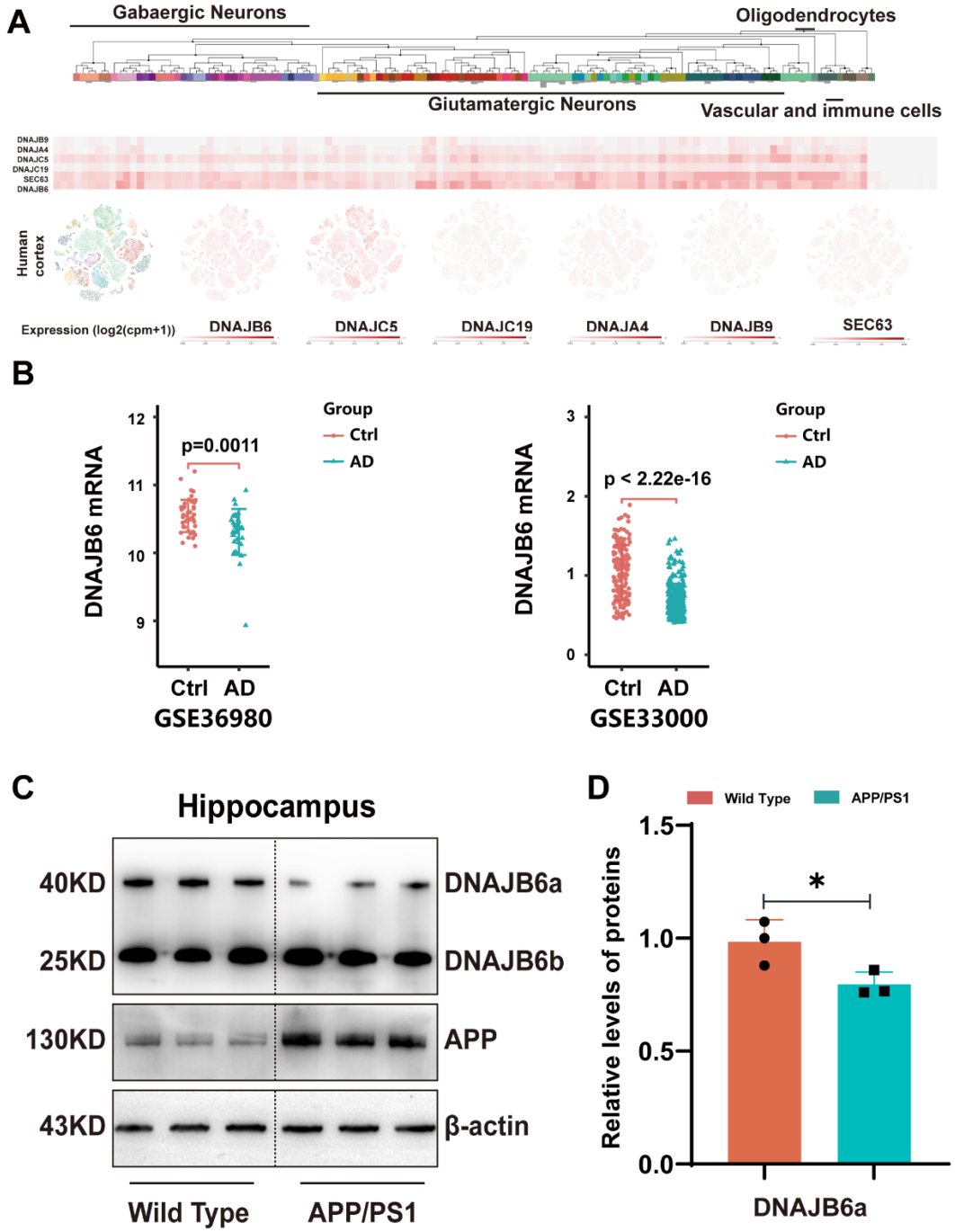

639

640 **Figure 1. DNAJB6a is downregulated in the brain of AD mice.**

641 (**A**) Single-cell RNA sequencing (Allen Institute for Brain Science) of sorted mouse

642 cortical and hippocampal neurons were mined for expression levels of HSP40. (**B**)

643 Differential expression gene analysis: DNAJB6 expression between AD and no-AD

644 controls (GSE36980: $p = 0.0011$; GSE3000: $p < 0.0001$). (**C-D**) Western blot analysis

Science Press
ZR Zoological Research

of the protein level of DNAJB6 in the hippocampus of 9-month-old APPswe/PS1dE9(APP/PS1) mice and the wild-type (WT) littermates (p = 0.0029). All data were expressed as mean ± SD. Data were considered significant if *$p < 0.05$, **$p < 0.01$, *** $p < 0.001$, ****$p < 0.0001$. Means were compared using the Student's t-test in panels **B-D.**

Science Press ZR Zoological Research

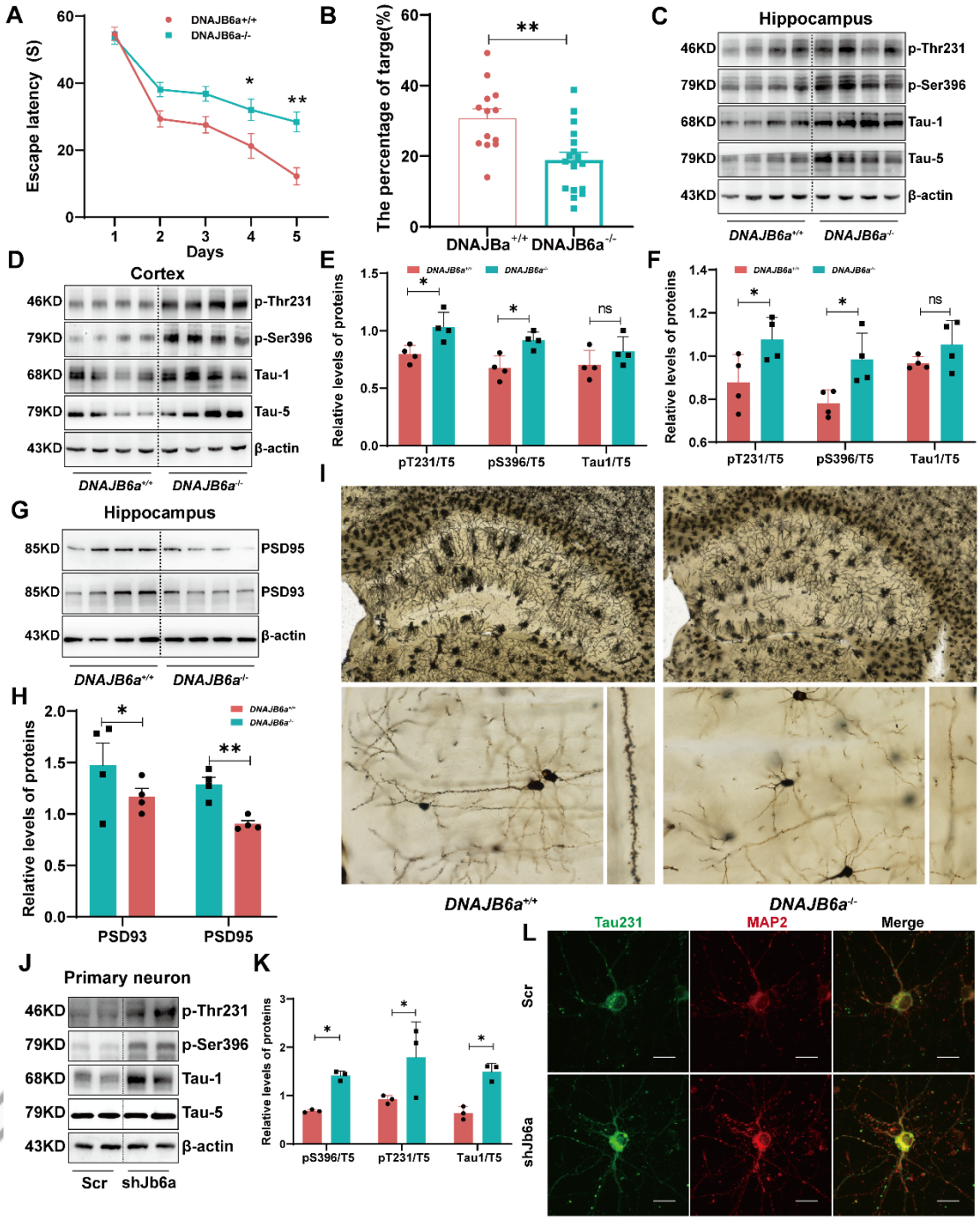

Figure 2. Tau hyperphosphorylation and impaired synaptic plasticity were observed in *DNAJB6a*$^{-/-}$ mice and DNAJB6a-shRNA neurons.

(**A**) Escape latency of 10-month-old DNAJB6a knockout mice (*DNAJB6a*$^{-/-}$) and the age-matched wild-type (*DNAJB6a*$^{+/+}$) littermates for 5 consecutive days in the MWM test. (**B**) The time percentage spent in the target quadrant in the spatial probe trial of

Science Press
ZR Zoological Research

672 the MWM test. (**C-F**) Western blot analysis of the level of p-Thr231, p-Ser396, and
673 Tau1, Tau-5 in the cortex and hippocampus of 10-month-old *DNAJB6a*$^{-/-}$ and the age-
674 matched wild-type *DNAJB6a*$^{+/+}$ littermates (p-Thr231/ Tau5 hippocampus: p =
675 0.0195; p-Ser396/ Tau5 hippocampus: p = 0.0164; Tau1/ Tau5 hippocampus: p =
676 0.3675; p-Thr231/ Tau5 cortex: p =0.0314; p-Ser396/ Tau5 cortex: p =0.0280; Tau1/
677 Tau5 cortex: p = 0.5558). (**G-H**) Western blot analysis of the level of PSD93 and
678 PSD95 in the hippocampus of *DNAJB6a*$^{+/+}$ and *DNAJB6a* $^{-/-}$ mice (PSD93/
679 hippocampus: p = 0.0141; PSD95/ hippocampus: p = 0.0012). (**I**) Representative
680 images of Golgi staining of hippocampus from 10-month-old *DNAJB6a*$^{+/+}$ and
681 *DNAJB6a*$^{-/-}$ mice. Selected dendritic segments from the hippocampus were
682 skeletonized using ImageJ software and analyzed. (**J-K**) Western blot analysis of the
683 level of p-Thr231, p-Ser396, and Tau1, Tau-5 in primary neuron cells transfected with
684 Scr or shJb6a (p-Thr231/Tau5: p = 0.0174; p-Ser396/ Tau5: p = 0.0465; Tau1/ Tau5:
685 p = 0.0200). (**L**) Primary neuron cells transfected with Scr or shJb6a were
686 coimmunostained for MAP2 (red) and phosphorylated (p)-Thr 231 tau (green).
687 All data were expressed as mean ± SD. **A-L** (n = 4 *DNAJB6a*$^{+/+}$; n= 4 *DNAJB6a* $^{-/-}$).
688 Data were considered significant if *p < 0.05, **p < 0.01, ***p < 0.001, ****p <
689 0.0001. Means were compared using the Student's t-test in panels **A-L**.
690 Scr: control lentivirus; shJb6a: shDNAJB6a lentivirus.
691
692
693

Science Press
ZR Zoological Research

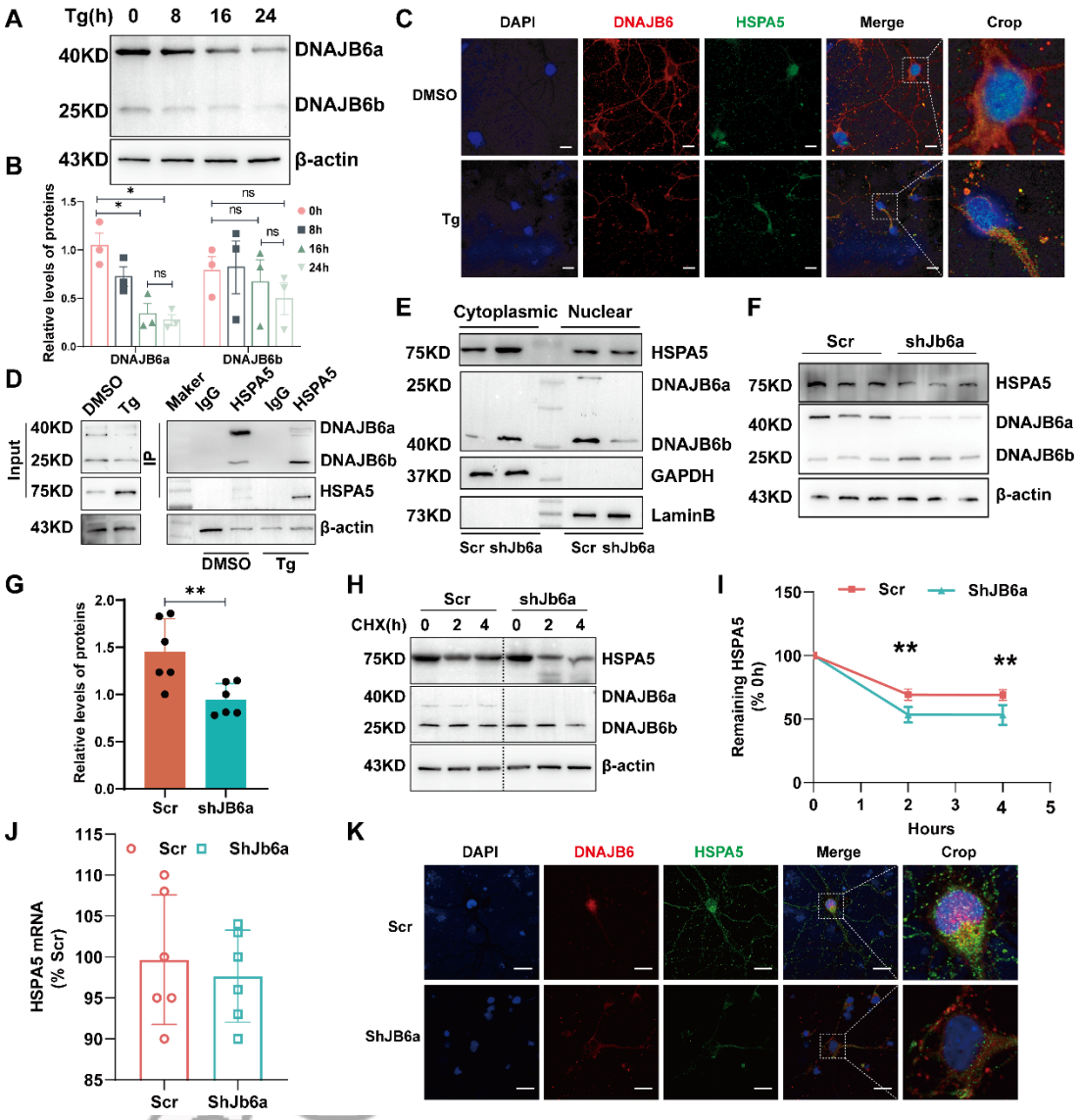

694

695 **Figure 3. DNAJB6a responded to ER stress via the regulation of HSPA5.**

696 (**A-B**) Western blot analysis of the level of DNAJB6 in primary neuron treated with
697 TG (Thapsigargin, 1 μM) for 0h, 8h, 16h, and 24h (DNAJB6a 0h vs. 16h: p = 0.0465;
698 DNAJB6a 0h vs. 24h: p = 0.0266). (**C**) Primary neuron cells treated with DMSO or
699 thapsigargin (Tg) were coimmunostained for DNAJB6 (red) and HSPA5 (green).
700 Scale bar: 20 μm. (**D**) Co-immunoprecipitation (CoIP) assay analysis of the
701 interaction between DNAJB6 and HSPA in primary neurons treated DMSO or Tg. (**E-**
702 **G**) Western blot analysis of the level of HSPA5 in primary neurons transfected with

Scr or shJb6a (p = 0.0098). (**H-I**) Western blot analysis of the level of HSPA5 in primary neurons transfected with Scr or shJb6a (CHX, 100 mg/mL) (2h: p = 0.0046; 4h: p = 0.0049). (**J**) Quantification of HSPA5 mRNA by qRT-PCR in primary neurons transfected with Scr or shJb6a (p = 0.0.6245). (**K**) Primary neuron cells transfected with Scr or shJb6a were coimmunostained for DNAJB6 (red) and HSPA5 (green). Scale bar: 20 μm.

All data were expressed as mean ± SD. **A-G**, **I** (n = 3 mice/group). Data were considered significant if *$p < 0.05$, **$p < 0.01$, ***$p < 0.001$, ****$p < 0.0001$. Means were compared using the Student's t-test.

Science Press ZR Zoological Research

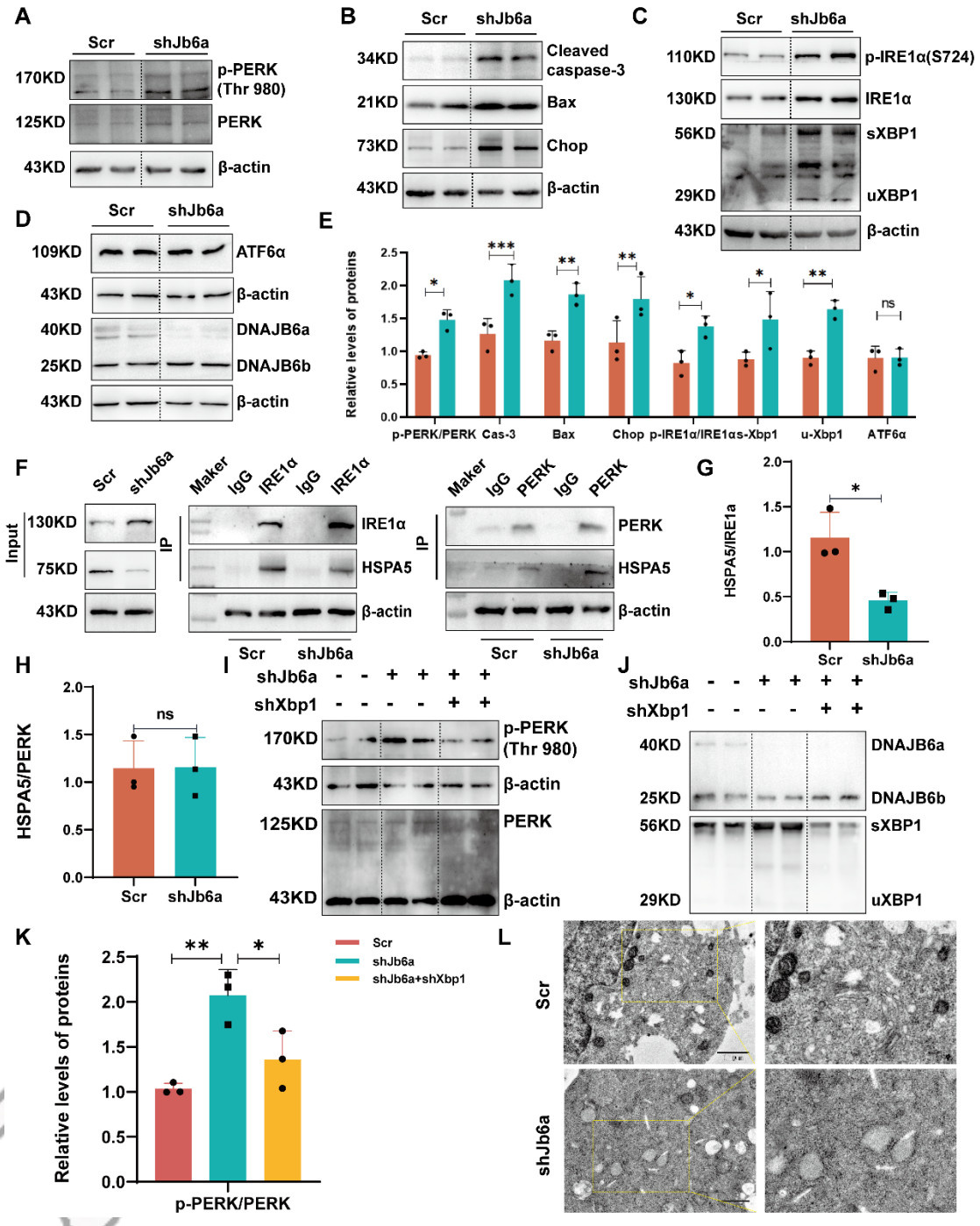

725

726 **Figure 4. DNAJB6a deficiency dysregulates PERK, IRE1α UPR branches.**

727 (**A-E**) Western blot analysis of the level of p-PERK, PERK, Cleaved-caspase-3, Bax,

728 Chop, p-IRE1α, IRE1α, XBP1, ATF6α in primary neurons transfected with Scr or

729 shJb6a (p-PERK/PERK: p = 0.0330; Cleaved-caspase-3: p = 0.0040; Bax: p = 0.0027,

730 Chop: p =0.0049, p-IRE1α/ IRE1α: p = 0.1618; s-Xbp1 ： p = 0.00124; u-Xbp1 ： p =

0.0015). (**F-H**) Co-immunoprecipitation (CoIP) assay analyzes the interaction of IRE1α or PERK and HSPA5 in primary neurons transfected with Scr or shJb6a (HSA5/IRE1α: p = 0.0433; HSA5/PERK: p = 0.9876). (**I-K**) Western blot analysis of the level of p-PERK, PERK in primary neurons transfected with Scr, shJb6a, shXbp1 (p-PERK Scr vs. shJb6a: p = 0.0069; p-PERK shJb6a vs. shJb6a+shXbp1: p = 0.0166). (**L**) Cultured primary neurons were transfected with Scr or shJb6a and then processed for EM visualization of the ER morphology. (Scale bar: 1μm).

All data were expressed as mean ± SD. **A-K** (n = 3 mice/group). Data were considered significant if *p < 0.05, **p < 0.01, ***p < 0.001, **** p< 0.0001. Means were compared using the Student's t-test in panels **A-H** and the One-way ANOVA test in panels **I-K.**

shXbp1: shXbp1 lentivirus

Science Press ZR Zoological Research

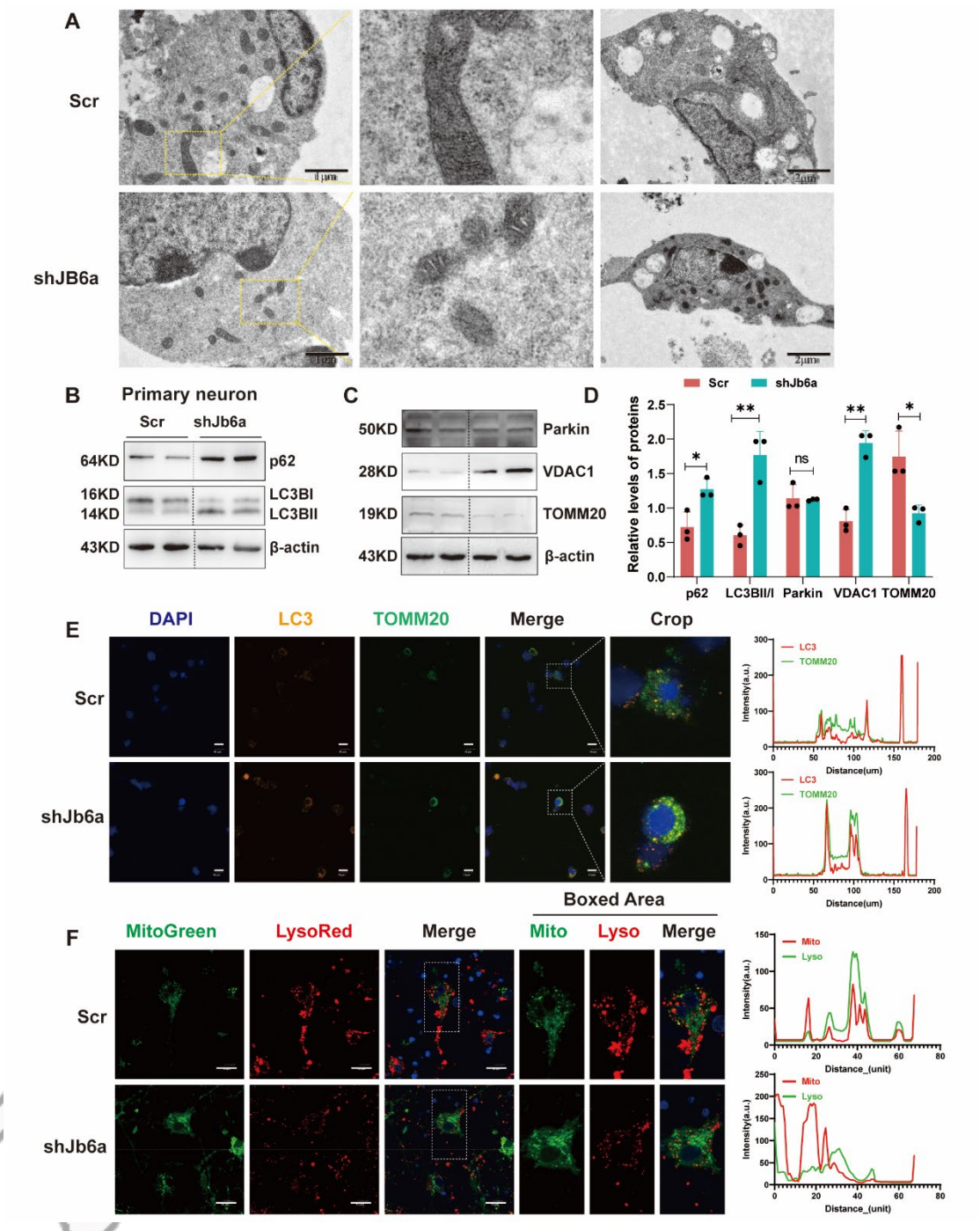

Figure 5. DNAJB6a deficiency hinders mitophagy by impairing mitochondrial and lysosomal fusion.

(**A**) Cultured primary neurons were transfected with Scr or shJb6a and then processed for EM visualization of the mitochondria. (Scale bar: 1μm). (**B-D**) Western blot analysis of the level of LC3, p62 Parkin, VDAC1, and TOMM20 in primary neurons

transfected with Scr or shJb6a (p62: p = 0.0225; LC3II/LC3I: p = 0.0058; VDAC1: p = 0.0144; TOMM20: p = 0.0210). (**E**) Primary neuron cells transfected with Scr or shJb6a were coimmunostained for LC3 (yellow) and TOMM20 (green). Scale bar: 20 μm. (**F**) Primary neuron cells transfected with Scr or shJb6a were coimmunostained for MitTracker (green) and LysoTracker(red). Scale bar: 20 μm. using the Student's *t*-test in panels **B**-**D**.

All data were expressed as mean ± SD. **B-D** (n = 3 mice/group). Data were considered significant if $*p < 0.05$, $**p < 0.01$, $***p < 0.001$, $****p < 0.0001$. Means were compared using the Student's t-test in panels **B-D**

Science Press ZR Zoological Research

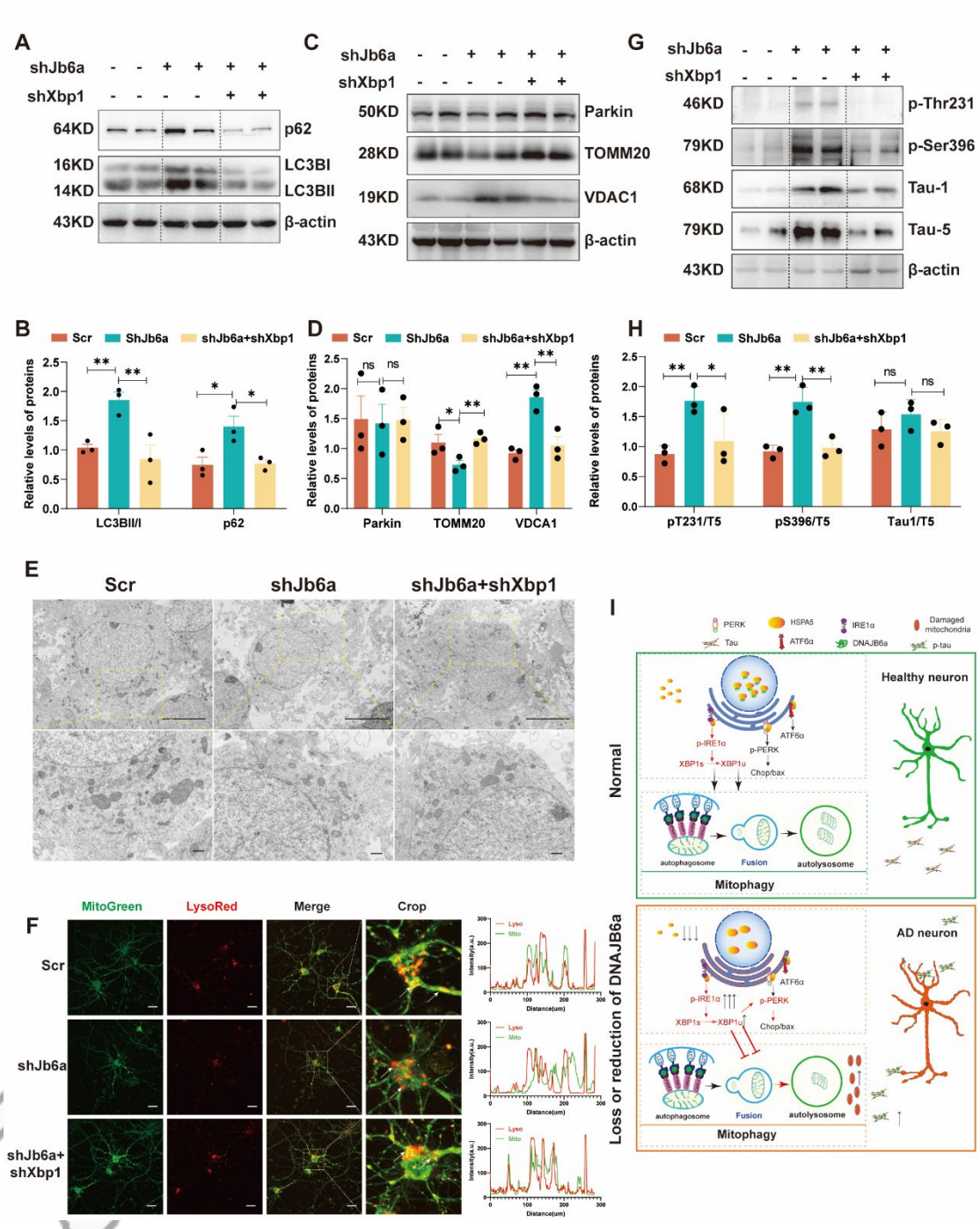

Figure 6. Xbp1 knockdown could rescue mitophagy deficiency and tau hyperphosphorylation induced by the deletion of DNAJB6a

(**A-B**) Western blot analysis of the level of LC3, p62 in primary neurons transfected with Scr, DNAJB6a-shRNA or DNAJB6a-shRNA+Xbp1-shRNA (p62 Scr vs. shJb6a: $p = 0.0067$; shJb6a vs. shJb6a+shXbp1: $p = 0.0017$). (**C-D**) Western blot analysis of

the level of Parkin, VDAC1, and TOMM20 in primary neurons transfected with Scr, DNAJB6a-shRNA or DNAJB6a-shRNA+Xbp1-shRNA (TOMM20 Scr vs. shJb6a: p = 0.0487; shJb6a vs. shJb6a+shXbp1: p = 0.0030; VDAC1 Scr vs. shJb6a: p = 0.0015; shJb6a vs. shJb6a+shXbp1: p = 0.0037). (**E**) Cultured primary neurons were transfected with Scr, DNAJB6a-shRNA or DNAJB6a-shRNA+Xbp1-shRNA and then processed for EM visualization of the mitochondria. (Scale bar: 5μm). (**F**) Containing MitTracker (green) with LysoTracker (red) in primary neurons transfected with Scr. DNAJB6a-shRNA or DNAJB6a-shRNA+Xbp1-shRNA. (**G-H**) Western blot analysis of the level of p-Thr231, p-Ser396, and Tau1, Tau-5 in primary neurons transfected with Scr, DNAJB6a-shRNA or DNAJB6a-shRNA+Xbp1-shRNA (p-Thr231/Tau5 Scr vs. shJb6a: p = 0.0011; shJb6a vs. shJb6a+shXbp1: p = 0.0111; p-Ser396/Tau5: Scr vs. shJb6a: p =0.0023; shJb6a vs. shJb6a+shXbp1: p = 0.0042; Tau1/Tau5 Scr vs. shJb6a: p = 0.4552; shJb6a vs. shJb6a+shXbp1: p = 0.3688). (**I**) Graphic abstract.

All data were expressed as mean ± SD. **A-F** (n = 3 mice/group). Data were considered significant if $*p < 0.05$, $**p < 0.01$, $***p < 0.001$, $****p < 0.0001$. Means were compared using the One-way ANOVA test in panels **A-C**

Science Press ZR Zoological Research

DNAJB6a 缺乏通过 IRE1α-Xbp1 诱导的线粒体功能障碍诱导 tau 病理

陈秀[1]，钱方媛[1]，赵娜[1]，刘雪婷，王燕娟，耿帆，朱萌萌，张志珺，任庆国*

东南大学医学院中大医院神经内科，江苏省脑科学与医学重点实验室，南京，210009，中国

摘要

内质网应激和线粒体自噬已被证实与阿尔茨海默病的早期病理进程相关，其中 tau 蛋白过度磷酸化是主要的病理改变之一，但其具体机制尚不明确。本研究识别出一种关键蛋白——DnaJ（Hsp40）同源蛋白 B 亚家族成员 6a（DNAJB6a），并阐明了其在阿尔茨海默病中的潜在致病作用。通过生物信息学方法对 DNAJB6 基因进行系统性筛选，证实其在阿尔茨海默病患者脑组织中表达降低。与对照组相比，APP/PS1 小鼠脑内 DNAJB6a 水平同样出现下降。DNAJB6a 基因敲除小鼠表现出认知功能障碍、突触缺失及阿尔茨海默病典型病理表型。DNAJB6a 缺失通过下调 70kDa 热休克蛋白 5（HSPA5）激活内质网应激通路。进一步研究发现，DNAJB6a 缺陷通过激活 IRE1α-XBP1 通路诱导线粒体功能障碍，从而加速阿尔茨海默病样表型的发生发展。这些发现表明，DNAJB6a 可能成为预防阿尔茨海默病病理进展的关键潜在靶点。

关键词：DNAJB6；IRE1α-Xbp1；阿尔茨海默病；线粒体自噬；tau 蛋白

Science Press ZR Zoological Research